Chemosphere 258 (2020) 127349

Contents lists available at ScienceDirect

Chemosphere

journal homepage: www.elsevier.com/locate/chemosphere

# Integration of subcellular partitioning and chemical forms to understand silver nanoparticles toxicity to lettuce (*Lactuca sativa* L.) under different exposure pathways

Wei-Qi Li [a, 1], Ting Qing [a, 1], Cheng-Cheng Li [a, b, *], Feng Li [a], Fei Ge [a], Jun-Jie Fei [b], Willie J.G.M. Peijnenburg [c, d]

[a] Department of Environmental Science and Engineering, College of Environment and Resources, Xiangtan University, Xiangtan, 411105, PR China
[b] Key Laboratory of Environmentally Friendly Chemistry and Applications of Ministry of Education, College of Chemistry, Xiangtan University, Xiangtan, 411105, PR China
[c] Institute of Environmental Sciences (CML), Leiden University, P.O. Box 9518, 2300, RA Leiden, the Netherlands
[d] National Institute of Public Health and the Environment (RIVM), P.O. Box 1, Bilthoven, the Netherlands

## HIGHLIGHTS

- This is the first study on subcellular and chemical forms partitioning of AgNPs *in planta* under different exposure pathway.
- Lettuce has higher tolerance to AgNP following foliar exposure than via root exposure.
- AgNP sequestration in metal-rich granules and heat stable fractions could best explain the AgNP tolerance.
- Low Ag proportion in inorganic form was potentially associated with AgNPs tolerance.
- Silver-containing NPs of 23.7 −39.4 nm were detected *in planta* by spICP-MS analysis.

## GRAPHICAL ABSTRACT

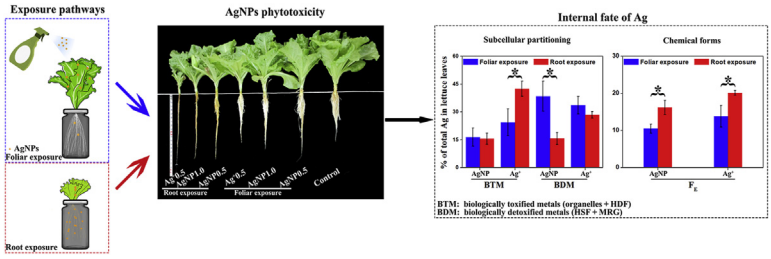


## ARTICLE INFO

*Article history:*
Received 7 January 2020
Received in revised form
3 June 2020
Accepted 5 June 2020
Available online 7 June 2020

Handling Editor: Tamara S. Galloway

## ABSTRACT

The current understanding of the biological impacts of silver nanoparticles (AgNPs) is restricted to the direct interactions of the particles with biota. Very little is known about their intracellular fate and subsequent toxic consequences. In this research we investigated the uptake, internal fate (i,e., Ag subcellular partitioning and chemical forms), and phytotoxicity of AgNPs in lettuce following foliar versus root exposure. At the same AgNP exposure concentrations, root exposure led to more deleterious effects than foliar exposure as evidenced by a larger extent of reduced plant biomass, elevated oxidative damage, as well as a higher amount of ultrastructural injuries, despite foliar exposure leading to 2.6−7.6 times more Ag bioaccumulation. Both Ag subcellular partitioning and chemical forms present within the plant appeared to elucidate this difference in toxicity. Following foliar exposure, high Ag in biologically

* Corresponding author. Department of Environmental Science and Engineering, College of Environment and Resources, Xiangtan University, Xiangtan, 411105, PR China.
*E-mail address:* ccli@xtu.edu.cn (C.-C. Li).
[1] Wei-Qi Li and Ting Qing are co-first authors who contributed equally to this work.

https://doi.org/10.1016/j.chemosphere.2020.127349

*Keywords:*
AgNPs
Phytotoxicity
Subcellular distribution
Chemical fraction
Foliar exposure
Root exposure

detoxified metals pool (29.2−53.0% by foliar exposure vs. 12.8−45.4% by root exposure) and low Ag proportion in inorganic form (6.1−11.9% vs. 14.1−19.8%) potentially associated with AgNPs tolerance. Silver-containing NPs (24.8−38.6 nm, 1.5−2.3 times larger than the initial size) were detected in lettuce plants exposed to NPs and to dissolved $Ag^{+}$, suggesting possible transformation and/or aggregation of AgNPs in the plants. Our observations show that the exposure pathway significantly affects the uptake and internal fate of AgNPs, and thus the associated phytotoxicity. The results are an important contribution to improve risk assessment of NPs, and will be critical to ensure food security.



## 1. Introduction

Silver nanoparticles (AgNPs) have found widespread application in consumer products, medicine, technology etc., amongst others due to their strong antimicrobial properties (Garner and Keller, 2014). Their growing use and production inevitably lead to an increased release into the environment and raise concerns about their environmental fate and toxicity (McGillicuddy et al., 2017). The appearance and buildup of engineered AgNPs in soil are likely via biosolids fertilization, irrigation and atmospheric deposition (Mueller and Nowack, 2008; He and Feng, 2017). The use of sewage sludge could contribute to an input of 1 μg AgNPs $kg^{-3}$ to agricultural soil per year (Mueller and Nowack, 2008). According to dynamic probabilistic modeling, the concentration of AgNPs will be up to 15.6 μg $kg^{-1}$ in sludge treated soil and 0.09 μg $kg^{-1}$ in natural and urban soil in 2020 in the EU (Sun et al., 2016). Moreover, AgNPs have extensively been tested for agriculture applications as plant protection products, including their use as pesticide or fungicide in recent years (Velu et al., 2017; Lowry et al., 2019). Consequently, a dramatically increased input of AgNPs to agricultural land is expected for the near future. Hence, there is an urgent need to improve evaluation of the risks of AgNPs in agricultural land.

Crops are a fundamental component of agroecosystems, which affect the fate and transport of NPs through plant uptake and accumulation (Monica and Cremonini, 2009). NPs accumulate in plants via either root or foliar uptake. AgNPs uptake by root has been extensively investigated (Yin et al., 2011; Schwab et al., 2016), whereas studies on foliar uptake of NPs are lagging behind. Furthermore, AgNPs are sprayed directly on crop plants as an antimicrobial agent used in agriculture (Kim et al., 2012; Lowry et al., 2019). Studies on the foliar exposure pathway are therefore necessary for a comprehensive risk assessment of nanomaterials, especially in agricultural soils. In a previous study, we showed that foliar exposure to AgNPs resulted in increased Ag accumulation but less toxicity in *Glycine* max and *Oryza sativa* tissues than in case of root exposure (Li et al., 2017). Larue et al. (2014) reported that foliar exposure to AgNPs caused detectable phytotoxicity symptoms to *Lactuca sativa* (Larue et al., 2014). These results, as well as those of earlier studies on $CeO_2$ NPs (Birbaum et al., 2010) and $TiO_2$ NPs (Larue et al., 2012) demonstrated the importance of the uptake pathways in the adverse impacts of NPs to plants. However, current knowledge regarding the exposure-pathway-specific bioaccumulation and phytotoxicity of NPs is still in its infancy.

In particular, it is still unclear whether toxicity is specifically associated with the subcellular compartmentalization and internal speciation of NPs *in planta* after NPs internalization via foliar uptake by cuticular and stomatal pathways (Avellan et al., 2019) or via root uptake by, e.g., endocytosis and wounds (Schwab et al., 2016). A pioneering formulation of the impacts of intracellular metal detoxification and bio-compartmentalization on cell viability, is the subcellular partitioning model (SPM) (William et al., 2003). According to this conceptual scheme, intracellular metal species are operationally classified as a spatial pool containing biologically detoxified (or inactive) metals (BDM) and another pool of biologically toxic (or active) metals (BTM). The sequestration of metal in the BDM and BTM pools relates to detoxification and harmful biological effects, respectively. An understanding of the metal subcellular localization and interaction to organelles and/or ligands in plants is critical to evaluating and mitigating its potential adverse ecological impacts. Indeed, Lan et al. (2019) found that more than 90% of the internalized Cd was located in the cell wall, which explained why *Microsorum pteropus* is a Cd hyperaccumulator (Lan et al., 2019). Similar results were also found in *Canna indica* L., as the majority of internalized Cd was blocked by the cell walls, and this Cd proportion increased with increasing Cd exposure levels (Dong et al., 2019). In addition to the SPM, the metal chemical forms approach has been developed to predict metal toxicity to terrestrial plants (Wu et al., 2005). This approach quantifies the fate of metal within cells into six forms: (i) inorganic form, (ii) water soluble form, (iii) metal pectate and protein-bound form, (iv) metal phosphates form, (v) oxalate form and (vi) residual form (Farago and Pitt, 1977; Wu et al., 2005). There is evidence that metals binding to pectates, phosphates, oxalates and residuals are less toxic to terrestrial plants, while the other forms are markedly phytotoxicity (Farago and Pitt, 1977; Li et al., 2014). Nevertheless, most of the above work has been done using metal ions, with only a few studies on metal-based NPs. A previous study (Zhang and Wang, 2019) demonstrated a similar subcellular Ag distribution pattern in a phytoplankton *Euglena gracilis* after AgNPs and $AgNO_3$ exposure with >50% Ag being in the cellular debris fraction, followed by the MRG (metal-rich granules) and organelles fractions (14−23%), while a negligible amount of Ag was present in the HDF (heat-denaturable fractions) and HSF (heat-stable fractions, 0.2−3%). The result indicated that cellular partitioning of AgNPs in *Euglena gracilis* was probably mediated by their dissolved fraction (Zhang and Wang, 2019). The high retention of Ag in the cellular debris fraction was also observed in *Glycine* max after bulk, nanoparticle and ionic Ag exposure (Quah et al., 2015). In order to address the questions 1) how the exposure pathway affects subcellular compartmentalization and internal species of AgNPs *in planta*, and 2) to what extent does this intracellular Ag speciation contribute to toxicity, we here examine the uptake, phytotoxicity and internal Ag fate (i.e., subcelluar distribution and chemical forms of AgNPs) in the leafy crop *Lactuca sativa* following foliar and root exposure. It is expected that the study will provide insight on the relationships between exposure pathway and phytotoxicity, and possible transformations of AgNPs *in planta*.

## 2. Materials and methods

### 2.1. Nanoparticles

Polyvinylpyrrolidone (PVP)-coated silver nanoparticles (AgNPs) were purchased from XFNANO Ltd. (Nanjing, China). The

morphology and particle size of the AgNPs in Milli-Q water (100 μg $mL^{-1}$ at pH 5.5 ± 0.1) were measured by transmission electron microscopy (TEM, Hitachi HT-7700, Japan) at 200 keV. The hydrodynamic diameter and zeta potential of AgNPs in Milli-Q water (1 μg $mL^{-1}$ at pH 5.5 ± 0.1) were measured by a zetasizer Nano instrument (Nano ZS, Zen 3700, Malvern Instruments, UK). AgNP suspensions were ultra-sonicated before experiments for 30 min to obtain a uniformly distributed solution.

### 2.2. Lettuce exposure

Lettuce (*Lactuca sativa* L. *var. ramosa Hort*) seeds purchased from a local seed company were surface-sterilized with 1% NaClO for 30 min and rinsed thoroughly with DI (deionized) water. They were then germinated on a moistened filter for 2 days in dark at 18 °C and 75% relative humidity, and then cultured with Hoagland solution (1.5 mM $KNO_3$, 2.0 mM $MgSO_4 \cdot 7H_2O$, 1.0 mM $Ca(NO)_3 \cdot 4H_2O$, 2.0 μM $(NH_4)_2HPO_4$, 0.016 μM Mo, 46 μM B, 0.32 μM Cu, 20.1 μM Fe, 0.77 μM Zn, and 9.1 μM Mn, pH 5.5 ± 0.1) for 42 days at 25 ± 1 °C and 16: 8 h light: dark photoperiod (375 μmol photon $m^{-2}$ $s^{-1}$).

The exposure experiment set three variables: species (PVP-AgNPs and $AgNO_3$), concentration and exposure pathway (root or foliar exposure) of Ag. The total treatment groups were as follows: Control, Foliar_NP0.5, Foliar_NP1.0, Foliar_$Ag^+$0.5, Root_NP0.5, Root_NP1.0, Root_$Ag^+$0.5 (Table S1). Each treatment combination was performed in triplicate.

#### 2.2.1. Foliar exposure

Freshly prepared AgNPs (0.5 or 1.0 mg $L^{-1}$) or $AgNO_3$ (0.5 mg $L^{-1}$) in DI water was sprayed onto lettuce leaves with acid-washed polypropylene sprayers with less than 19% loss of adsorbed Ag. To confirm foliar Ag was the only source, an impervious membrane was used to block penetration of the spray solution into the pots: no Ag was detected in the pots at the end of the experiment. Each lettuce was sprayed three times a day with 100 mL of the exposure suspension for 7 days (Li et al., 2017). Control treatments with DI water were also set up. After exposure, the lettuce roots and leaves (the 3rd-5th leaves from lettuce apex) were collected for analysis.

#### 2.2.2. Root exposure

Lettuce seedlings were exposed to AgNPs (0.5 or 1.0 mg $L^{-1}$) or $AgNO_3$ (0.5 mg $L^{-1}$) in Hoagland solution as described above. The exposure solution was replenished every day. The lettuce leaves and roots were harvested and weighed separately after 7 consecutive days of exposure. The lettuce roots and leaves (the 3rd-5th leaves from apex) were washed with flowing ultrapure water, $HNO_3$ (10 mM), l-cysteine (10 mM, freshly prepared) and finally with ultrapure water to remove loosely bound AgNPs/Ag ions (removal rate: 82.6 ± 2.2%) for further analysis.

### 2.3. Ultrastructure of plant cells

#### 2.3.1. Morphological analysis by transmission electron microscope

Lettuce leaves were sliced into 1 mm × 1 mm sized parts and double-fixed in 2.5% glutaraldehyde solution with Millonig's phosphate buffer (MPB, pH 7.3) and fixed overnight at ambient temperature. Specimens were washed three times at 10 min intervals with MPB, incubated for 1 h in 1% osmium tetroxide, and dehydrated in a gradient ethanol series (30%, 50%, 70%, and 100%) for 30 min for each step (Gonçalves et al., 2018). They were then soaked in a 1: 1 mix of acetone: resin for 12 h and 100% resin to polymerize overnight at 37 °C, and then another 12 h at 60 °C. After double staining with 3% uranyl acetate and lead nitrate, the specimens were sliced (50–100 nm thickness) and examined by transmission electron microscope (TEM, Hitachi, HT-7700, Japan) at an accelerating voltage of 80 kV (Tang et al., 2017).

#### 2.3.2. Morphological analysis by atomic force microscopy

Thylakoids were isolated before atomic force microscopy (AFM) measurements (Rintamäki et al., 1996). The leave tissue was homogenized in buffer A (300 mM sucrose, 50 mM Hepes-NaOH, 10 mM NaF, 5 mM $MgCl_2$, 1 mM $Na_2$-EDTA, pH 7.5), filtered through two layers of gauze, and centrifuged at 1500 g for 4 min. The resulting pellet was re-suspended and washed with buffer B (5 mM sucrose, 10 mM Hepes-NaOH, 10 mM NaF, 5 mM $MgCl_2$, pH 7.5) and centrifuged (3000 g, 3 min). The thylakoid membrane was suspended in buffer C (100 mM sucrose, 10 mM Hepes-NaOH, 5 mM NaCl, 10 mM NaF, 10 mM $MgCl_2$, pH 7.5), frozen with liquid nitrogen and stored at −80 °C until use. Imaging of isolated thylakoids was accomplished with AFM according to published procedures (Doltchinkova et al., 2019). The thylakoid volume was calculated based on the formula $V = (4\pi abh)/3$, where a, b and h were the length, width and the height of the thylakoid, respectively (Doltchinkova et al., 2019).

### 2.4. Biochemical assays

#### 2.4.1. Antioxidant enzyme assay

Lettuce tissues were homogenized mechanically (Ningbo Science Biotechnology, Ltd) in ice-cold buffer solution (1% Polyvinyl Pyrrolidone, 0.05 M $NaH_2PO_4/Na_2HPO_4$, pH 7.4), then centrifuged (10,000 g, 10 min). All operations were performed at 4 °C. The supernatant was used for the determination of superoxide dismutase superoxide dismutase (SOD) and catalase (CAT) activities. Catalase activity was determined by using a CAT assay kit (S0051, Beyotime Co., China) based on the method described by Fossati et al. (1980). The hydrogen peroxide ($H_2O_2$) consumed by CAT per minute at 25 °C was defined as CAT activity, which was expressed as unit $mg^{-1}$ fresh weight (FW). Superoxide dismutase activity was determined with a SOD assay kit (S0109, Beyotime Co., China) based on the nitroblue tetrazolium (NBT) method described by Beauchamp and Fridovich (1971). The amount of enzyme required to cause 50% inhibition of the rate of NBT chloride reduction was defined as SOD activity, which was expressed as unit $mg^{-1}$ FW.

#### 2.4.2. Lipid peroxidation determination

Malondialdehyde (MDA) contents were measured by a thiobarbituric acid (TBA) reactive substances (TBARS) assay according to the protocol provided by Jambunathan and Niranjani (Jambunathan, 2010). Briefly, 0.5 g of lettuce tissue was homogenized in trichloroacetic acid (0.1%, 4 mL) and then centrifuged at a high speed (10,000 g, 15 min, 4 °C). The supernatant (1 mL), along with trichloroacetic acid (20%, 2 mL) and TBA (0.5%, 3 mL) were mixed thoroughly, and then heated in a 95 °C water bath for 30 min before subjected to UV absorbance analysis at 532 nm and 600 nm (Cary 60 UV–Vis spectrophotometer, Agilent Technologies). The experimental results were presented as μmol $\mu g^{-1}$ FW.

#### 2.4.3. Hydrogen peroxide ($H_2O_2$) analysis

The $H_2O_2$ concentration was estimated according to the modified protocol of Brennan and Frenkel (1977). Briefly, 0.5 g of lettuce tissues were homogenized with acetone (1 mL) and centrifuged (3000 g, 10 min, 4 °C). Then, titanic sulfate (5%, 0.1 mL) and concentrated ammonium hydroxide (0.2 mL) were added to the supernatant (1 mL) successively to form peroxide-titanium complex precipitate. The precipitate was measured at 415 nm (Cary 60 UV–Vis spectrophotometer, Agilent Technologies, USA) after washing with acetone for three times and solubilizing in sulfuric

acid (1 M, 5 mL). The results were presented as μmol $g^{-1}$ FW.

### 2.5. Internal Ag subcellular partitioning and chemical forms

#### 2.5.1. Subcellular distribution

Determination of metal subcellular partitioning *in planta* was based on the method used in previous studies (Lavoie et al., 2009). A total of five parts were separated:

(1) cellular debris, comprising cell walls, cell membranes and nuclei;
(2) metal-rich granules (MRG), NaOH-resistant or granule-like fraction;
(3) organelles, a subcellular part combining various organelles, e.g. Golgi apparatus, mitochondria;
(4) heat-stable fractions (HSF), involving glutathione (GSH), metallothioneins and phytochelatins;
(5) heat-denaturable fractions (HDF), e.g. enzymes.

Briefly, lettuce leaves (~0.2 g) were homogenized with buffer solution (10 mL) containing dithioerythritol (1 mM), sucrose (25 mM), and Tris–HCl (50 mM, pH 7.5, Fisher Scientific). After the first centrifugation (2500 g, 15 min, 4 °C), the precipitate was suspended in deionized water (2 mL) and heated in water bath (100 °C, 2 min), then digested with NaOH (1.0 M, 2 mL) in another water bath (70 °C, 1 h), and centrifuged (10,000 g, 15 min, 4 °C) to separate the supernatant (cellular debris) and pellet (metal-rich granules, MRG). The supernatant was then centrifuged (100,000 g, 1 h, 4 °C) to sediment the organelles components. The remaining supernatant was kept in a water bath (80 °C, 10 min) and then cooled for 1 h on ice, centrifuged for another time (50,000 g, 30 min, 4 °C) to separate the supernatant (heat-stable fractions, HSF) and pellet (heat-denaturable fractions, HDF).

#### 2.5.2. Distribution of chemical forms

The determination of the chemical forms was carried out according to previously reported methods (Wu et al., 2005; Li et al., 2014). Frozen lettuce leaves (~2 g) were homogenized with extraction solution (30 mL) in centrifugation tubes. Silver in different chemical forms were extracted in the order as follows:

$F_E$, 80% ethanol, extracting Ag giving priority to nitrite, nitrate, some amino acids, and low molecular compounds (inorganic form); $F_W$, deionized water, extracting water-soluble Ag of organic acid and metaphosphate (water soluble form); $F_{NaCl}$, 1 M NaCl, extracting Ag associated with pectates and proteins (pectate and protein-bound form); $F_{HAC}$, 2% HAC, extracting undissolved Ag bound to phosphate (phosphates form); $F_{HCl}$, 0.6 M HCl, extracting Ag associated with oxalate (oxalate form); $F_R$, Ag in the form of residual states (residual form).

After shaking (120 rpm, 22 h, and 25 °C), the homogenate was centrifuged (5000 g, 10 min). The precipitate was re-suspended in the same extraction solution and shaken for another 2 h as described above. After centrifugation (5000 g, 10 min), the supernatant was pooled for Ag analysis.

### 2.6. Ag determination

#### 2.6.1. Total Ag

Total Ag in lettuce was analyzed using ICP-MS (Agilent, 7700x, USA), after the tissues were freeze-dried and digested in a 1: 4 (v: v) mixture of $H_2O_2$ and $HNO_3$. Citrus leaf (GBW 10020, certified reference material, Chinese Academy of Geophysical Sciences) was concurrently digested. The Ag recovery rates were 96.2 ± 6.6%.

#### 2.6.2. Size distribution of AgNPs within leaves

Quantification of Ag-containing NPs size distribution in lettuce leaves was analyzed using single-particle (sp)ICP-MS (Agilent 8800, Agilent Technologies, USA) followed by Macerozyme R-10 digestion (Dan et al., 2015). Briefly, 0.1 g of lettuce leaves were homogenized with citrate buffer (8 mL, 2 mM, pH 6.0), then digested (37 °C, 36 h) after 0.1 g Macerozyme R-10 was added and settling for 1 h. After dilution, the supernatant was analyzed by spICP-MS with a size detection limit of 13.2 nm (Text S1, Table S2). For each sample, 20,000 data points were generated with an average dwell time of 0.1 ms and an acquisition time of 60 s (Fig. S1). $^{107}Ag$ was monitored during the measurement. Transport efficiency (TE) was determined using 30 and 50 nm PVP-AgNPs (NanoComposix) based on the method of particle frequency under the same instrumental conditions (Dang et al., 2019). Calibration curves were generated using a nanoparticulate standard (30-, 50- and 80-nm PVP-AgNPs, NanoComposix) and an ionic standard ($AgNO_3$, Sigma).

### 2.7. Statistical analysis

Differences between treatments were tested using one-way ANOVA (SPSS 19.0), followed by Student–Newman–Keuls (S–N–K) tests at a significance of $p < 0.05$. Data was present as mean ± SD (n = 3).

## 3. Results and discussion

### 3.1. AgNPs characterization

Polyvinylpyrrolidone (PVP)-coated AgNPs in Milli-Q water (1 μg $mL^{-1}$ NPs, pH 5.5 ± 0.1) were spherical with an average hydrodynamic size of 63.0 ± 3.0 nm (Fig. 1A, B, C) and had a zeta potential of −18.6 ± 1.7 mV. The particle size measured by TEM was 16.5 ± 0.3 nm, comparable to the measurement result of spICP-MS (16.5 ± 0.2 nm) (Fig. 1D). The percentage of ion Ag in the AgNP suspensions (Hoagland solution, pH 5.5 ± 0.1) was 2.0–7.5% as determined by ultracentrifugation (Fig. S2).

### 3.2. Lower toxicity and higher Ag bioaccumulation following foliar exposure to AgNPs

The biomass and biochemical assays revealed exposure pathway-specific toxicity of AgNPs to lettuce. Generally, foliar exposure of AgNPs led to less toxicity to lettuce than root exposure. The fresh biomass decreased by 38.1–55.7% (leaves) and 29.6–47.5% (roots) following foliar application when compared with the control group (Fig. 2A). Under root exposure, the decline in biomass was more pronounced as leaves weight decreased by 62.2–84.0% and root weight by 63.2–83.7% (Fig. 2A). The results showed that growth inhibition was Ag species-independent and dose-nonspecific despite a decreasing trend of biomass with exposure dose and more biomass loss in the dissolved $Ag^+$ groups was noted (Fig. 2A). However, substantial differences ($p < 0.05$) were observed in the biochemical assays. Note that we use the 3rd-5th leaves from lettuce apex to do the biochemical assays to exclude the aging effects of plant. Particularly, hydrogen peroxide and MDA levels increased significantly as the AgNPs dose was increased in both the root and the foliar exposure pathways (Fig. 2B). Moreover, both $H_2O_2$ and MDA concentrations in the dissolved $Ag^+$ group were dramatically higher than in the NPs exposure treatment, indicating that $AgNO_3$ was more deleterious than AgNP at an identical total Ag concentration. These findings are consistent with other studies suggesting that AgNP toxicity was predominantly attributed to the release of $Ag^+$ (Pradas del Real et al., 2017), although particle-specific toxicity was also shown to

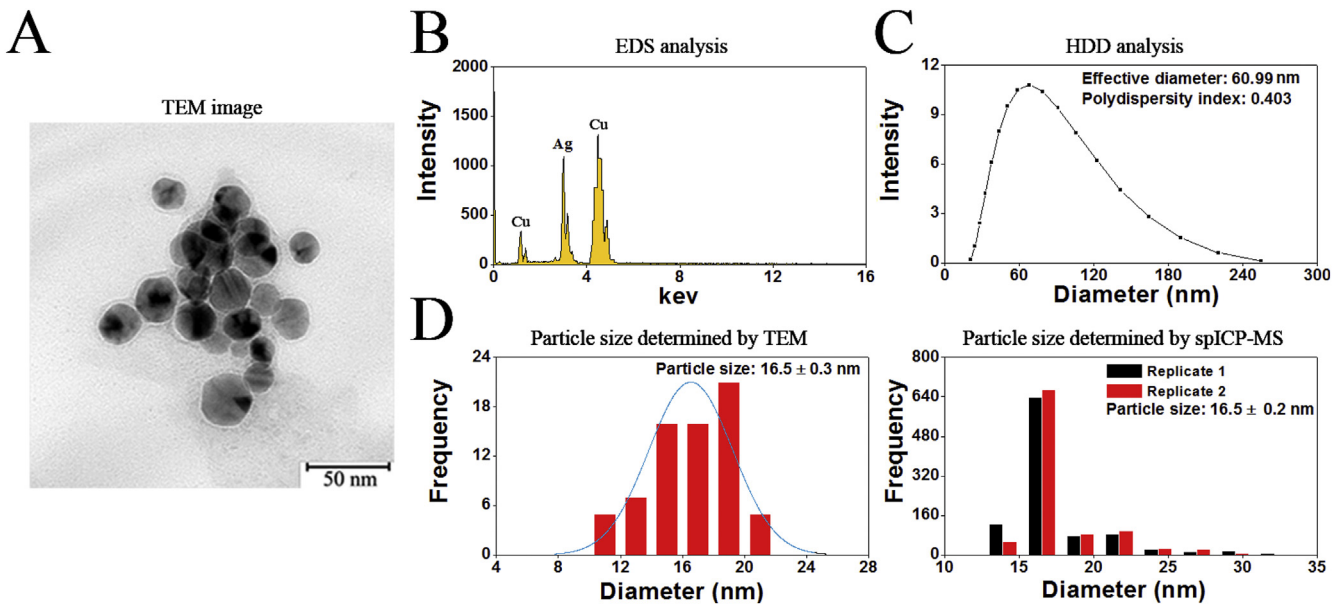


**Fig. 1.** Silver nanoparticle characterization. (A) Transmission electron microscopy (TEM) image, (B) energy dispersive X-ray spectroscopy (EDS) analysis, and (C) hydrodynamic diameter of AgNPs (pH 5.5 ± 0.1, 1 μg $mL^{-1}$) in Milli-Q water. (D) Comparison of particle size distribution of AgNPs as measured by TEM images and single-particle inductively coupled plasma mass spectrometry (spICP-MS).

be responsible for the effects observed (Gorka and Liu, 2016). The $H_2O_2$ and MDA contents in lettuce leaves were also higher when AgNPs exposed to roots, compared to foliar exposed group ($H_2O_2$: 660.2 ± 116.3 vs. 198.7 ± 10.2 μmol $g^{-1}$ for 0.5 mg AgNPs $L^{-1}$, 828.8 ± 106.0 vs. 378.0 ± 21.2 μmol $g^{-1}$ for 1.0 mg AgNPs $L^{-1}$; MDA: 5.2 ± 0.3 vs. 2.8 ± 0.1 μmol $\mu g^{-1}$ for 0.5 mg AgNPs $L^{-1}$, 5.3 ± 0.1 vs. 3.1 ± 0.2 μmol $\mu g^{-1}$ for 1.0 mg AgNPs $L^{-1}$, Fig. 2B), indicating that root exposure led to higher toxicity of AgNPs. The SOD and CAT activities, however, were less sensitive to AgNPs exposure, with enhanced levels consistently observed only in the Foliar_$Ag^{+}$0.5 and Root_NP1.0 treatments (Fig. 2B). No significant alteration of SOD and CAT activities were observed for the 0.5 mg AgNPs $L^{-1}$ treatment. These results suggested that responses of the antioxidant defense mechanism might vary upon NP exposure. Both SOD and CAT can specifically scavenge excessive amounts of reactive oxygen species (ROS) in plants. Moreover, ROS may disturb the gene expression of antioxidants and attack membrane lipids directly, which can be indicated by potential biomarkers of $H_2O_2$ and MDA (Ma et al., 2015). Therefore, the high content of $H_2O_2$ and MDA under root exposure of AgNPs justifies the increase of the observed antioxidant enzymes (SOD and CAT) activity. Thus, the enhanced ROS production might lead to cytotoxicity including plasmolysis, rupture of cell walls (Fig. 3A) as well as thylakoids membranes damage with shrinkage volume (Control, 351.0 $\mu m^3$ > Foliar_NP1.0, 68.2 $\mu m^3$ > Root_NP1.0, 51.3 $\mu m^3$) and distinct grana and lamella on the surface (Fig. 3B), subsequently inducing plant senescence and even death (Fig. S3–5). Bioaccumulation of Ag in lettuce was associated with the exposure pathway and the initial Ag species (NPs vs. $Ag^{+}$). In general, Ag accumulation in lettuce increased with increasing Ag exposure, within the range of 3.0–80.3 μg $g^{-1}$ DW. As expected, more Ag accumulated in lettuce via foliar than via root exposure (except for the $AgNO_3$ treatment), being 2.7-times higher and 6.6-times higher when exposed to AgNPs of 0.5 mg $L^{-1}$ and 1.0 mg $L^{-1}$, respectively. In addition, dissolved $Ag^{+}$ was more easily accumulated *in planta* than NPs at equivalent application levels, irrespective of the application route (62.3 ± 7.6 vs. 9.8 ± 0.1 μg $g^{-1}$ for foliar exposure, 77.5 ± 2.8 vs. 3.6 ± 0.2 μg $g^{-1}$ for root exposure, DW). Although there was measurable dissolved $Ag^{+}$ in 0.5 mg AgNP $L^{-1}$ suspensions (Fig. S2), its concentration was only 11.63 ± 2.46 μg $L^{-1}$ (over 37.0 times lower than the concentration in Root_$Ag^{+}$0.5 group), and similar results were also found in the foliar exposure suspensions. Thence, the accumulation of Ag cannot fully account by the ion Ag dissolved from AgNPs. Rather, accumulation of particle-specific Ag took place *in planta*.

It is well known that lettuce is a common leaf crop and its high accumulation of Ag poses a potential risk for human health through nutrient transfer. This study demonstrated that when selecting plants biomass, ultrastructural damages, $H_2O_2$ and MDA contents as key endpoints, AgNPs was more deleterious to the plants when applied to roots than to leaves. However, it is the foliar exposure pathway and not the root exposure pathway that was found to be more efficient in accumulating Ag, as should be taken into consideration in AgNP risks assessment. Potential reasons for these contrasting responses of lettuce to AgNPs taken up by roots and leaves were: (i) the differences of the fate of Ag *in planta* after foliar exposure or root exposure might lead to different toxicity; (ii) the physiological functions were different between leaves and roots during the growth of plants. For example, silver accumulated via root exposure directly acted on the lettuce roots and seriously affected root growth (Fig. S3), which in turn affected the whole physiological processes of plants (Yin et al., 2011); (iii) Ag detected in leaves after foliar exposure might contain both adsorbed and internalized absorbed Ag (Larue et al., 2014). In this study, we mainly focus on the acting mechanism of (i), and intracellular AgNPs transformation and fate (subcellular compartmentalization and internal species of NPs) are thus explored.

### 3.3. Mechanisms of lower phytotoxicity following foliar exposure

Differences in AgNP accumulation patterns in lettuce could be explained by the internal fate of Ag *in planta* (as determined by Ag subcellular partitioning and chemical forms). The subcellular partitioning model (SPM) displays important effects of exposure pathway on heavy metals bioaccumulation, migration, and toxicity in plants. Briefly, the metallic biological toxified metals (BTM, organelles + HDF) is the target of toxic action of metals, while the

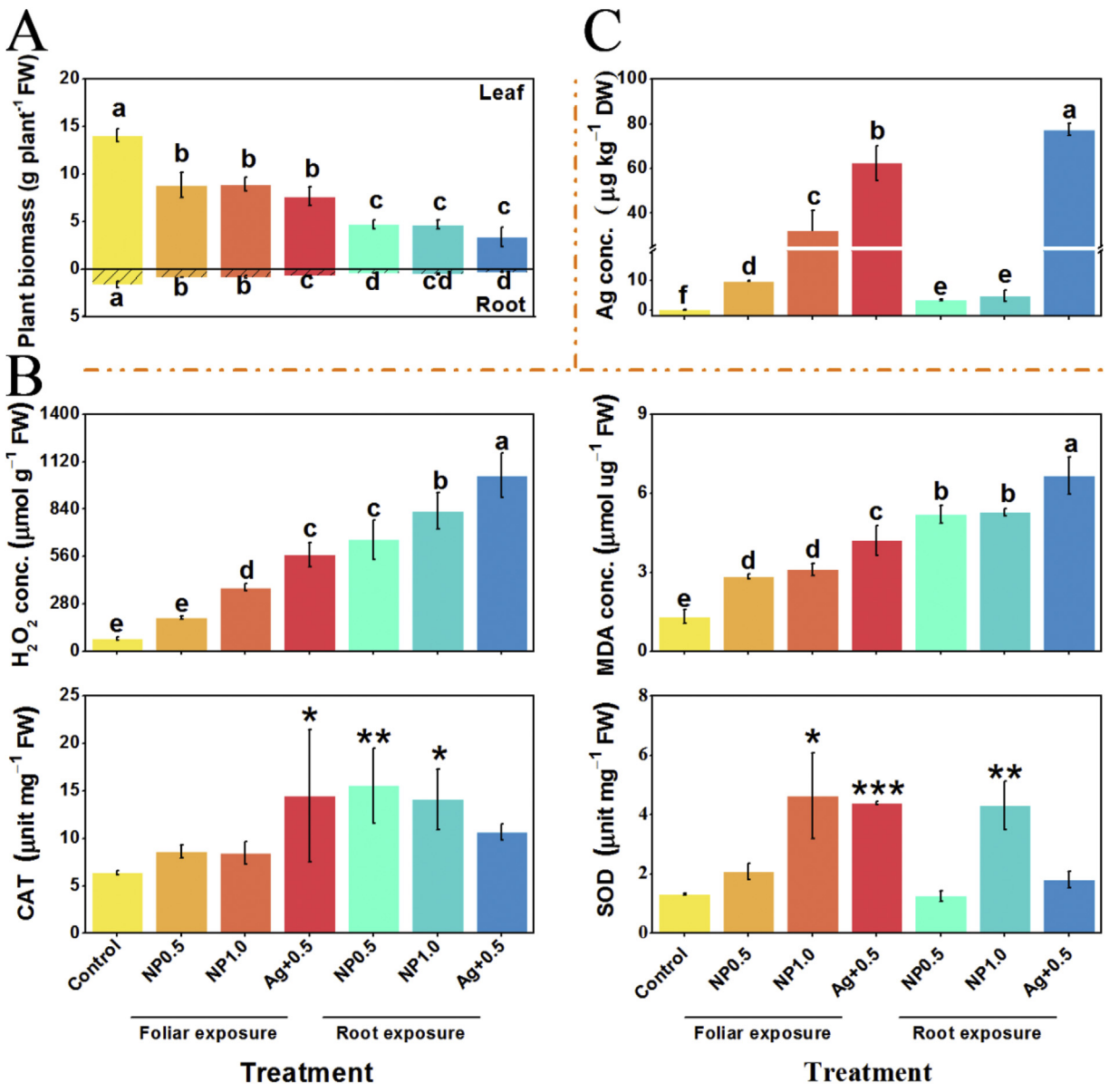


**Fig. 2.** Plant biomass, biochemical assays and Ag accumulation in lettuce after 7 days of exposure to AgNPs or dissolved $Ag^+$. (A) Plant biomass of lettuce seedlings. (B) $H_2O_2$, MDA contents, and CAT, SOD activities in lettuce leaves. (C) Silver concentrations in lettuce leaves. Data are the mean ± SD (n = 3). NP0.5, NP1.0 and $Ag^+$0.5 represent lettuce exposure to 0.5 mg AgNPs $L^{-1}$, 1.0 mg AgNPs $L^{-1}$ and 0.5 mg $Ag^+$ $L^{-1}$, respectively. * ($p < 0.05$), ** ($p < 0.01$) and *** ($p < 0.001$) indicate significant differences from control. Different letters represent statistical differences among treatments at $p < 0.05$.

biological detoxified metals (BDM, HSF + MRG) is believed to alleviate the metal toxicity. Indeed, in foliar exposed lettuce, more Ag was associated with the BDM (29.2–53.0%) than in root exposed lettuce (12.8–45.4%), whilst less Ag was associated with the BTM (11.8–31.0% in the foliar exposure group, compared to 13.7–46.6% in the root exposure group) (Fig. 4A). We are unaware of any previous study that found such divergence between exposure pathways. Overall, silver partitioning in the subcellular fractions were as follows: cellular debris (24.8–79.3%) > MRG (metal-rich granules, 9.4–52.5%) ≈ organelles (10.8–45.5%) > HSF (heat-stable fractions, 0.18–3.7%) ≈ HDF (heat-denatured fractions, 0.4–4.0%) (Fig. 4A). It is interesting to note, the cellular debris, constituted primarily by material of cell wall (Lavoie et al., 2009), showed a maximum Ag adsorption capacity in both exposure pathways. Cell wall-integrated metal was protective of the adverse effects to plants (Lan et al., 2019). The subcellular partitioning between foliar exposure and root exposure can also be distinguished by metal rich granules (MRG) and organelles fraction, which were reported to alleviate metal toxicity in phytoplankton (Lavoie et al., 2009). MRG and organelles accounted for 29.0–52.5% and 11.3–29.2% Ag retention for foliar exposure, and thus reduced Ag toxicity. In contrast, 9.4–44.1% intracellular Ag in MRG and 10.8–45.5% intracellular Ag in organelles of root exposed plants suggested potential toxicity. Thus, SPM provides a biological relevant framework for understanding the insensitivity to Ag in case of foliar exposure under a high NP exposure level. Typically, the amount of Ag associated with MRG in the Foliar_NP1.0 group was 3.1-fold higher than in the Root_NP1.0 group, leading the former to have a proportion of Ag in the BDM (38.5 ± 8.1% vs. 15.7 ± 2.5%), where Ag is considered to be detoxified. We also found that the Ag in the BTM for the

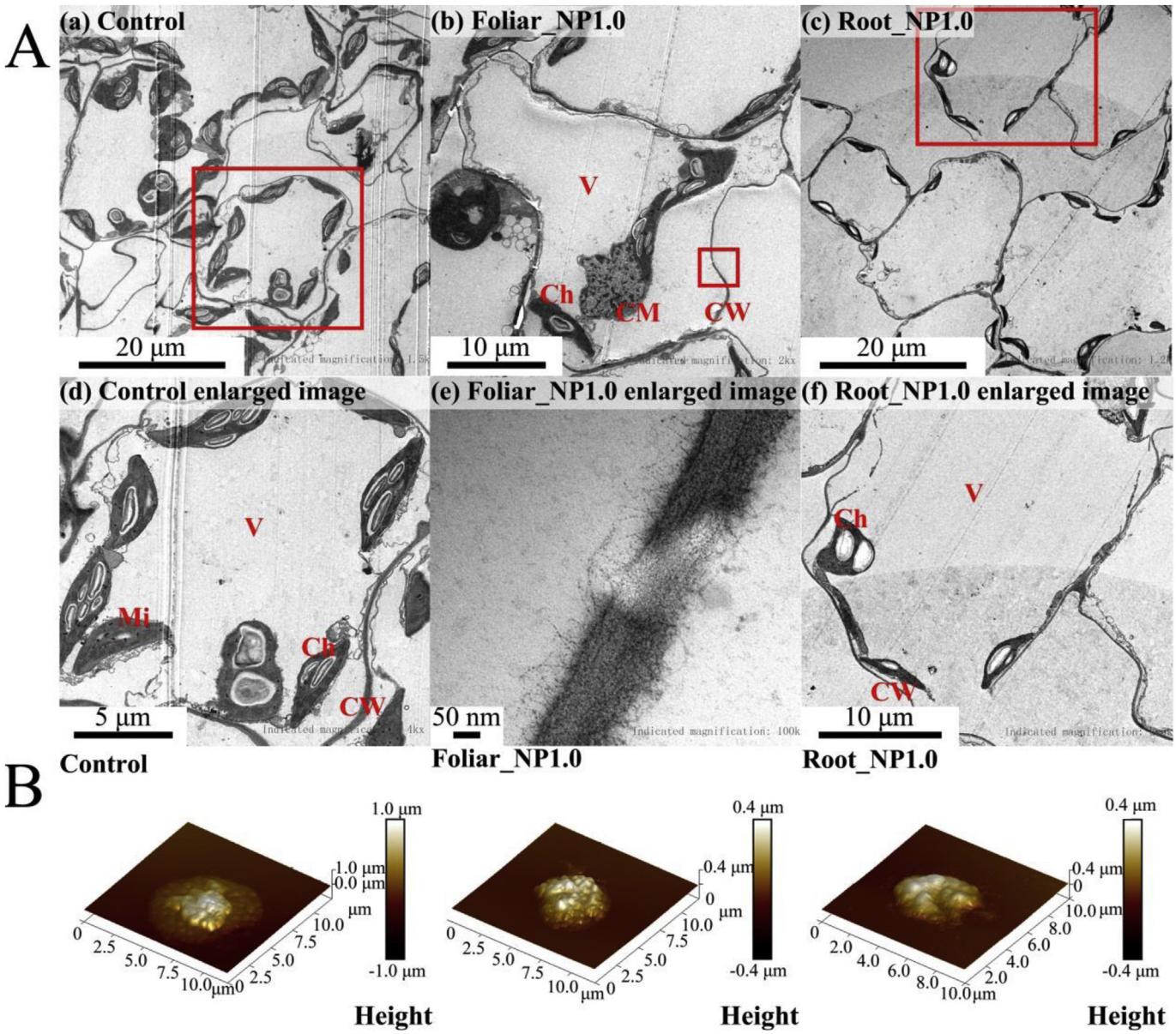


**Fig. 3.** Morphological analysis of lettuce leaves. (A) Transmission electron microscopy (TEM) images of lettuce leaves after 7 days of exposure to AgNPs. Plots d–f show an enlargement of the area inside the red rectangles in plots a–c, respectively. V: Vacuoles, Ch: Chloroplast, CW: Cell Wall, CM: Cell Membrane, Mi: Mitochondria. (B) Atomic force microscopy (AFM) of envelope-free thylakoids from lettuce cells after 7 days of exposure to 1.0 mg AgNPs $L^{-1}$. Volumes of thylakoids were calculated based on formula $V = (4\pi abh)/3$, where a, b and h were the length, width and the height of the thylakoid, respectively. The volume of thylakoids in the representative AFM images decreased in the order: Control (351.0 $\mu m^3$) > Foliar_NP1.0 (68.2 $\mu m^3$) > Root_NP1.0 (51.3 $\mu m^3$), suggesting the greater thylakoids damages by AgNP via root exposure than foliar exposure. (For interpretation of the references to colour in this figure legend, the reader is referred to the Web version of this article.)

dissolved $Ag^+$ exposed group was >1.0–3.4 times higher than for the AgNPs group ($Ag^+$0.5 vs. NP0.5). Our results on Ag internal fate in lettuce thus indicate a clear nano-specific effect.

The approach based on the chemical form of a metal serves as an independent approach to understand the cellular fate of a metal. Metal in the inorganic and water soluble forms ($F_E + F_W$) was more toxic compared to the low active phosphate and oxalate form ($F_{HAc} + F_{HCl}$) (Li et al., 2014). The high active water soluble ($F_W$) and inorganic Ag forms ($F_E$) consisted mainly of $AgNO_3$, as well as Ag bound to dihydric phosphate and organic acids, which easily penetrate into the symplast and locate in cell organelles. They exhibit higher migratory capacity and have more negative effects on plant cells. In the present study, Ag chemical forms present within lettuce were investigated to elucidate AgNP toxicity difference under different exposure pathways. In lettuce, most of the Ag was distributed in the water soluble form (19.8–30.5%, $F_W$), the pectate and protein-bound form (13.0–29.8%, $F_{NaCl}$) and the oxalate form (7.9–36.7% of total Ag amount, $F_{HCl}$), followed by the inorganic form (6.1–20.8%, $F_E$), the phosphates form (4.2–20.4%, $F_{HAC}$), and the residual form (0.6–13.7%, $F_R$) (Fig. 4B). AgNPs in the inorganic form in lettuce following root exposure accounted for 14.1–19.8% of the total internalized Ag, which was 1.9 times higher than Ag (6.1–11.9%) in the foliar exposure group (Fig. 4B), despite the water-soluble Ag distributed comparably *in planta*. This disparity was more pronounced in NP0.5 group (17.0 ± 2.7% vs. 6.5 ± 0.7%), as root exposed lettuce accumulated more than 2.6 times higher Ag than foliar exposed lettuce (Fig. 4B). It is reasonable to interpret that root application of AgNPs is recommended as a

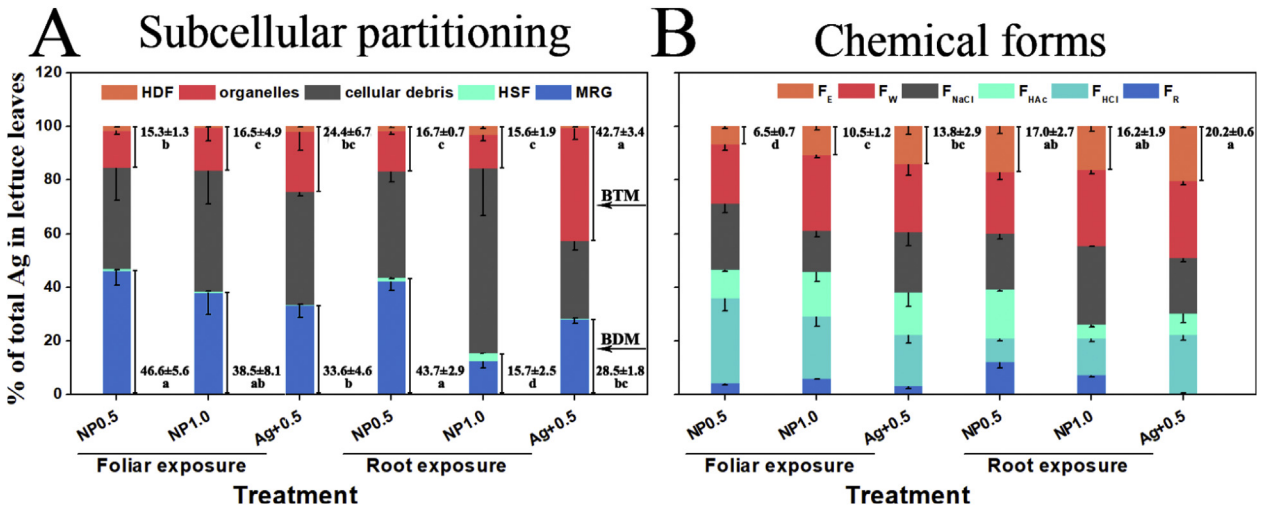


**Fig. 4.** Subcellular distribution and chemical forms of Ag in lettuce. (A) Subcellular proportions of Ag in the leaves of lettuce after 7 days of exposure to AgNPs or dissolved $Ag^+$. Silver in each subcellular fraction is expressed as percentage of total Ag in the lettuce. Subcellular compartments are as follows: cellular debris, MRG: metal-rich granules, organelles, HSF: heat-stable fractions, HDF: heat-denaturable fractions. Biologically toxic metals (BTM) and biologically detoxified metals (BDM) are present as red and blue segments, respectively. (B) Chemical forms proportions of Ag in the leaves of lettuce after 7 days exposure to AgNPs or dissolved $Ag^+$. Silver in each chemical form is expressed as percentage of total Ag in the lettuce. Silver in different chemical forms are as follows: $F_E$: inorganic form, $F_W$: water soluble form, $F_{NaCl}$: pectate and protein-bound form, $F_{HAC}$: silver phosphates form, $F_{HCl}$: silver oxalate form, $F_R$: residual form. Values are mean ± SD (n = 3). Different letters indicate a significant difference at $p < 0.05$ among the different treatments. (For interpretation of the references to colour in this figure legend, the reader is referred to the Web version of this article.)

more plant-damaging exposure way. The pectate and protein-bound form was one of the main Ag forms *in planta*. Cell wall, mainly comprised of polyoses, proteins and pectins, providing abundant ligands (e.g., carboxyl, hydroxyl) for metal chelation, therefore, some pectate and protein-bound Ag may be located in plants cell walls (Haynes, 1980). Thus, from a chemical forms perspective, the cell wall serves an important protective mechanism to AgNP exposure, which was consistent with the results obtained by SPM (showing that 28.9–68.7% Ag was retained by the cell wall). As a result, cell walls improve the plant tolerance by insulating the protoplasts from AgNP outside (Krzesłowska et al., 2016). In the present research, we explained the diversity of accumulation and toxicity *in planta* following different exposure pathways through the practical tool of subcellular partitioning model and the chemical forms approach. And a further study is needed to analyze the migration process of Ag *in planta* for better evaluating the risks of AgNPs in ecosystem.

### 3.4. Size distributions of Ag-containing particles in planta following foliar and root exposure

Ag-containing NPs were detected in lettuce leaves regardless of exposure pathway and Ag species (NPs vs. dissolved $Ag^+$), and these *in planta* NPs (24.8–38.6 nm) were significantly larger than

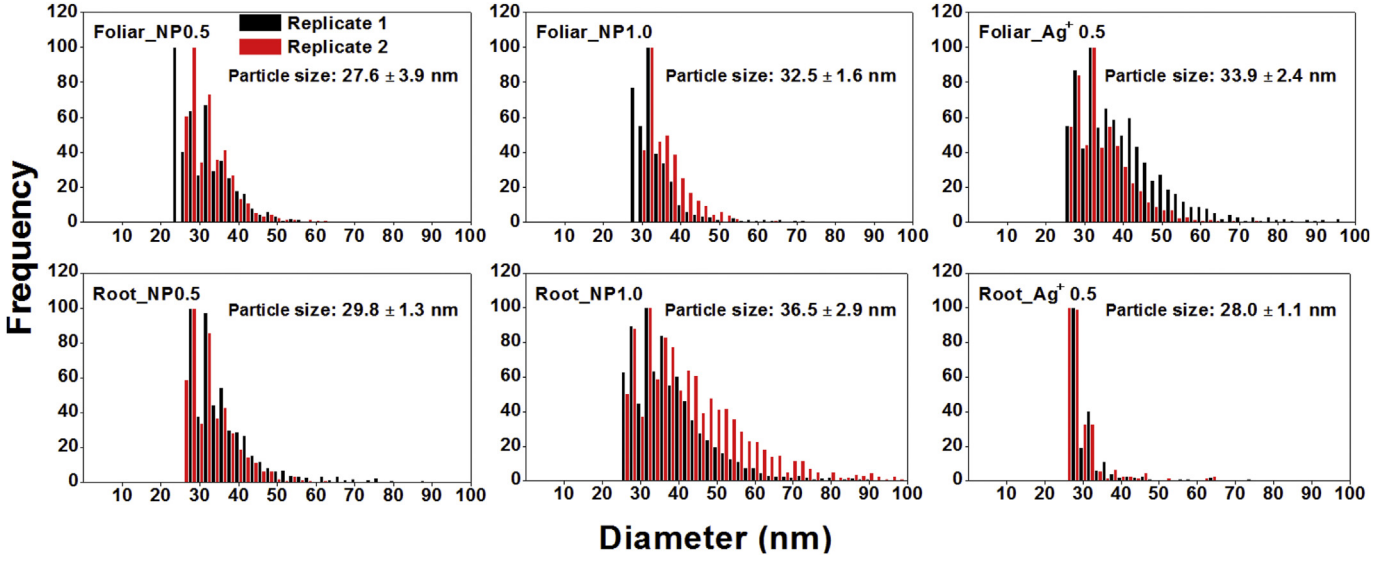


**Fig. 5.** Particle size distribution of Ag-containing NPs within lettuce. Representative particle size distribution histograms of Ag-containing NPs in lettuce leaves exposed to AgNPs or dissolved $Ag^+$ via foliar exposure or root exposure. Data for two replicates are presented.

the pristine AgNPs (16.5 ± 0.2 nm) (Figs. 1D and 5). This is probably a result of bio-dissolution and transformation. Quantifying the size changes of NPs is essential to understanding the biological toxicity and ecological risks of NPs, since particle size was found to markedly affect the biological effects of NPs (Wang et al., 2016). Previous studies found that AgNP toxicity was influenced by particle size with smaller AgNPs (6 nm) inhibiting plant growth more than did identical concentrations of larger (25 nm) NPs (Yin et al., 2011). Similarly, Falco et al. (2020) found that the adverse effects on the photosynthetic activity to *Vicia faba* by AgNPs was increasing with decreasing particle size (Falco et al., 2020). Moreover, particle size could also affect the adhesion of NPs on the wheat leaves, as the percentage of 3 nm AuNPs adhesion to leaves was almost twice than that of 10 nm (Avellan et al., 2019). Other studies have shown that the trophic transfer of gold nanoparticles from the producer (*Nicotiana tabacum* L. cv *Xanthi*) to a primary consumer (*Manduca sexta*) decreased with particle size increase (Judy et al., 2011). In the present study, comparable Ag-containing particles size distribution was found in lettuce leaves under root vs. foliar exposure (31.4 ± 4.3 nm vs. 31.3 ± 3.7 nm), and thus failed to interpret AgNP phytotoxicity difference under different exposure pathway by intracellular particle size distribution. Interestingly, in addition to the lettuce exposed to AgNPs, lettuce exposed to $AgNO_3$ also resulted in an average NPs size of 27.2–35.6 nm *in planta* (Fig. 5). Therefore, part of the Ag had been reduced to nanoparticles after taken up by plants. This *in planta* transformation may lead to potential trophic transfer of NPs since plants serve as the basis of terrestrial food webs.

## 4. Conclusion

These findings demonstrate that AgNP uptake, phytotoxicity, internal subcellular and chemical forms vary with exposure pathways. Compared to root exposure, foliar exposure leads to greater Ag accumulation but lower toxic impacts to plants. Both the Ag subcellular partitioning model and the chemical forms approach elucidated the toxicity difference, and highlight the key role of cell walls in lettuce tolerance to AgNP. Ag-containing NPs (24.8–38.6 nm) were detected within lettuce under AgNPs and dissolved $Ag^+$ exposure, and they are 1.5–2.3 times larger than the initial size (16.5 ± 0.2 nm), indicative of the possible transformations and/or aggregation of AgNPs. Further research is needed on the AgNPs transformation and chemical speciation *in planta* using *in situ* analytical techniques (e.g., XAS). Nevertheless, these results signal that the exposure pathway may affect the internal fate of AgNPs in lettuce, and they therefore affect the subsequent phytotoxicity of AgNPs. Our findings on the mechanistic basis for AgNPs toxicity differences between exposure pathways might benefit studies of NPs–plant interactions.

## Declaration of competing interest

The authors declare that they have no known competing financial interests or personal relationships that could have appeared to influence the work reported in this paper.

## CRediT authorship contribution statement

**Wei-Qi Li:** Methodology, Investigation, Data curation, Writing - original draft, Conceptualization, Software. **Ting Qing:** Writing - original draft, Conceptualization, Investigation, Formal analysis, Methodology, Data curation. **Cheng-Cheng Li:** Resources, Funding acquisition, Methodology, Supervision, Writing - review & editing. **Feng Li:** Software, Methodology, Validation. **Fei Ge:** Validation, Formal analysis, Writing - review & editing. **Jun-Jie Fei:** Writing - review & editing. **Willie J.G.M. Peijnenburg:** Writing - review & editing.

## Acknowledgements

We thank the National Natural Science Foundation of China (No. 41701580) and the Natural Science Foundation of Hunan Province (2019JJ50581) for funding this research. Part of this study was supported by the Key Laboratory of Soil Environment and Pollution Remediation, Institute of Soil Science, Chinese Academy of Sciences (SER 2017-05) as well as the China Postdoctoral Science Foundation Funded Project (2018M642992).

## Appendix A. Supplementary data

Supplementary data to this article can be found online at https://doi.org/10.1016/j.chemosphere.2020.127349.

## References

Avellan, A., Yun, J., Zhang, Y., Spielman-Sun, E., Unrine, J.M., Thieme, J., Li, J., Lombi, E., Bland, G., Lowry, G.V., 2019. Nanoparticle size and coating chemistry control foliar uptake pathways, translocation, and leaf-to-rhizosphere transport in wheat. ACS Nano 13, 5291–5305.

Beauchamp, C., Fridovich, I., 1971. Superoxide dismutase: improved assays and an assay applicable to acrylamide gels. Anal. Biochem. 44, 276–287.

Birbaum, K., Brogioli, R., Schellenberg, M., Martinoia, E., Stark, W.J., Günther, D., Limbach, L.K., 2010. No evidence for cerium dioxide nanoparticle translocation in maize plants. Environ. Sci. Technol. 44, 8718–8723.

Brennan, T., Frenkel, C., 1977. Involvement of hydrogen peroxide in the regulation of senescence in pear. Plant Physiol. 59, 411–416.

Dan, Y., Zhang, W., Xue, R., Ma, X., Stephan, C., Shi, H., 2015. Characterization of gold nanoparticle uptake by tomato plants using enzymatic extraction followed by single-particle inductively coupled plasma–mass spectrometry analysis. Environ. Sci. Technol. 49, 3007–3014.

Dang, F., Chen, Y.Z., Huang, Y.N., Hintelmann, H., Si, Y.B., Zhou, D.M., 2019. Discerning the sources of silver nanoparticle in a terrestrial food chain by stable isotope tracer technique. Environ. Sci. Technol. 3802–3810.

Doltchinkova, V., Andreeva, T., Georgieva, K., Mihailova, G., Balashev, K., 2019. Desiccation-induced alterations in surface topography of thylakoids from resurrection plant *Haberlea rhodopensis* studied by atomic force microscopy, electrokinetic and optical measurements. Physiol. Plantarum 166, 585–595.

Dong, X., Yang, F., Yang, S., Yan, C., 2019. Subcellular distribution and tolerance of cadmium in *Canna indica* L. Ecotox. Environ. Safe. 185, 109692.

Falco, W.F., Scherer, M.D., Oliveira, S.L., Wender, H., Colbeck, I., Lawson, T., Caires, A.R.L., 2020. Phytotoxicity of silver nanoparticles on *Vicia faba*: evaluation of particle size effects on photosynthetic performance and leaf gas exchange. Sci. Total Environ. 701, 134816.

Farago, M.E., Pitt, M.J., 1977. Plants which accumulate metals. Part II. An investigation of the soluble zinc containing extracts from two australian species. Inorg. Chim. Acta. 24, 127–130.

Fossati, P., Prencipe, L., Berti, G., 1980. Use of 3,5-dichloro-2-hydroxybenzenesulfonic acid/4-aminophenazone chromogenic system in direct enzymic assay of uric acid in serum and urine. Clin. Chem. 26, 227.

Garner, K.L., Keller, A.A., 2014. Emerging patterns for engineered nanomaterials in the environment: a review of fate and toxicity studies. J. Nano Res. 16, 2503.

Gonçalves, C.S., Ávila, A.R., de Souza, W., Motta, M.C.M., Cavalcanti, D.P., 2018. Revisiting the *Trypanosoma cruzi* metacyclogenesis: morphological and ultrastructural analyses during cell differentiation. Parasites Vectors 11, 83.

Gorka, D.E., Liu, J., 2016. Effect of direct contact on the phytotoxicity of silver nanomaterials. Environ. Sci. Technol. 50, 10370–10376.

Haynes, R., 1980. Ion exchange properties of roots and ionic interactions within the root apoplasm: their role in ion accumulation by plants. Bot. Rev. 46, 75–99.

He, S., Feng, Y., 2017. The impact of engineered nanomaterials on crops and soil microorganisms. In: Prasad, R., Kumar, V., Kumar, M. (Eds.), Nanotechnology: Food and Environmental Paradigm. Springer Singapore, Singapore, pp. 191–208.

Jambunathan, N., 2010. Determination and detection of reactive oxygen species (ROS), lipid peroxidation, and electrolyte leakage in plants. In: Sunkar, R. (Ed.), Plant Stress Tolerance: Methods and Protocols. Humana Press, Totowa, NJ, pp. 291–297.

Judy, J.D., Unrine, J.M., Bertsch, P.M., 2011. Evidence for biomagnification of gold nanoparticles within a terrestrial food chain. Environ. Sci. Technol. 45, 776–781.

Kim, S.W., Jung, J.H., Lamsal, K., Kim, Y.S., Min, J.S., Lee, Y.S., 2012. Antifungal effects of silver nanoparticles (AgNPs) against various plant pathogenic fungi. MYCOBIOLOGY 40, 53–58.

Krzesłowska, M., Rabęda, I., Basińska, A., Lewandowski, M., Mellerowicz, E.J., Napieralska, A., Samardakiewicz, S., Woźny, A., 2016. Pectinous cell wall thickenings formation – a common defense strategy of plants to cope with Pb.

Environ. Pollut. 214, 354–361.
Lan, X.Y., Yan, Y.Y., Yang, B., Li, X.Y., Xu, F.L., 2019. Subcellular distribution of cadmium in a novel potential aquatic hyperaccumulator – *Microsorum pteropus*. Environ. Pollut. 248, 1020–1027.
Larue, C., Castillo-Michel, H., Sobanska, S., Cécillon, L., Bureau, S., Barthès, V., Ouerdane, L., Carrière, M., Sarret, G., 2014. Foliar exposure of the crop *Lactuca sativa* to silver nanoparticles: evidence for internalization and changes in Ag speciation. J. Hazard Mater. 264, 98–106.
Larue, C., Veronesi, G., Flank, A.-M., Surble, S., Herlin-Boime, N., Carrière, M., 2012. Comparative uptake and impact of $TiO_2$ nanoparticles in wheat and rapeseed. J. Toxicol. Environ. Health A 75, 722–734.
Lavoie, M., Le Faucheur, S., Fortin, C., Campbell, P.G.C., 2009. Cadmium detoxification strategies in two phytoplankton species: metal binding by newly synthesized thiolated peptides and metal sequestration in granules. Aquat. Toxicol. 92, 65–75.
Li, C.C., Dang, F., Cang, L., Zhou, C.F., Zhou, D.M., 2014. Integration of metal chemical forms and subcellular partitioning to understand metal toxicity in two lettuce (*Lactuca sativa* L.) cultivars. Plant Soil 384, 201–212.
Li, C.C., Dang, F., Li, M., Zhu, M., Zhong, H., Hintelmann, H., Zhou, D.M., 2017. Effects of exposure pathways on the accumulation and phytotoxicity of silver nanoparticles in soybean and rice. Nanotoxicology 11, 699–709.
Lowry, G.V., Avellan, A., Gilbertson, L.M., 2019. Opportunities and challenges for nanotechnology in the agri-tech revolution. Nat. Nanotechnol. 14, 517–522.
Ma, C., White, J.C., Dhankher, O.P., Xing, B., 2015. Metal-based nanotoxicity and detoxification pathways in higher plants. Environ. Sci. Technol. 49, 7109–7122.
McGillicuddy, E., Murray, I., Kavanagh, S., Morrison, L., Fogarty, A., Cormican, M., Dockery, P., Prendergast, M., Rowan, N., Morris, D., 2017. Silver nanoparticles in the environment: sources, detection and ecotoxicology. Sci. Total Environ. 575, 231–246.
Monica, R.C., Cremonini, R., 2009. Nanoparticles and higher plants. Caryologia 62, 161–165.
Mueller, N.C., Nowack, B., 2008. Exposure modeling of engineered nanoparticles in the environment. Environ. Sci. Technol. 42, 4447–4453.
Pradas del Real, A.E., Vidal, V., Carrière, M., Castillo-Michel, H., Levard, C., Chaurand, P., Sarret, G., 2017. Silver nanoparticles and wheat roots: a complex interplay. Environ. Sci. Technol. 51, 5774–5782.
Quah, B., Musante, C., White, J.C., Ma, X., 2015. Phytotoxicity, uptake, and accumulation of silver with different particle sizes and chemical forms. J. Nano Res. 17, 277.
Rintamäki, E., Salo, R., Koivuniemi, A., Aro, E.M., 1996. Protein phosphorylation and magnesium status regulate the degradation of the D1 reaction centre protein of Photosystem II. Plant Sci. 115, 175–182.
Schwab, F., Zhai, G., Kern, M., Turner, A., Schnoor, J.L., Wiesner, M.R., 2016. Barriers, pathways and processes for uptake, translocation and accumulation of nanomaterials in plants – critical review. Nanotoxicology 10, 257–278.
Sun, T.Y., Bornhöft, N.A., Hungerbühler, K., Nowack, B., 2016. Dynamic probabilistic modeling of environmental emissions of engineered nanomaterials. Environ. Sci. Technol. 50, 4701–4711.
Tang, J., Zhu, N., Zhu, Y., Liu, J., Wu, C., Kerr, P., Wu, Y., Lam, P.K.S., 2017. Responses of periphyton to $Fe_2O_3$ nanoparticles: a physiological and ecological basis for defending nanotoxicity. Environ. Sci. Technol. 51, 10797–10805.
Velu, M., Lee, J.H., Chang, W.S., Lovanh, N., Park, Y.J., Jayanthi, P., Palanivel, V., Oh, B.T., 2017. Fabrication, optimization, and characterization of noble silver nanoparticles from sugarcane leaf (*Saccharum officinarum*) extract for antifungal application. 3 Biotech 7, 147.
Wang, P., Lombi, E., Zhao, F.J., Kopittke, P.M., 2016. Nanotechnology: a new opportunity in plant sciences. Trends Plant Sci. 21, 699–712.
William, G.W., Byeong-Gweon, L., Samuel, N.L., 2003. Subcellular compartmentalization of Cd and Zn in two bivalves. I. Significance of metal-sensitive fractions (MSF) and biologically detoxified metal (BDM). Mar. Ecol. Prog. Ser. 249, 183–197.
Wu, F.B., Dong, J., Qian, Q.Q., Zhang, G.P., 2005. Subcellular distribution and chemical form of Cd and Cd–Zn interaction in different barley genotypes. Chemosphere 60, 1437–1446.
Yin, L., Cheng, Y., Espinasse, B., Colman, B.P., Auffan, M., Wiesner, M., Rose, J., Liu, J., Bernhardt, E.S., 2011. More than the Ions: the effects of silver nanoparticles on *Lolium multiflorum*. Environ. Sci. Technol. 45, 2360–2367.
Zhang, L., Wang, W., 2019. Dominant role of silver ions in silver nanoparticle toxicity to a unicellular alga: evidence from luminogen imaging. Environ. Sci. Technol. 53, 494–502.